Available online at www.sciencedirect.com
SCIENCE DIRECT®
Continental Shelf Research 25 (2005) 753–773
CONTINENTAL SHELF RESEARCH
www.elsevier.com/locate/csr

Weak wind-wave/tide interaction over fixed and moveable bottoms: a formulation and some preliminary results

B.A. Kagan[a,*], O. Alvarez[b,c,1], A. Izquierdo[b]

[a]*Shirshov Institute of Oceanology, Russian Academy of Sciences, St. Petersburg Branch, 30 Pervaya Liniya, 199053 St. Petersburg, Russia*
[b]*Departamento de Fisica Aplicada, Universidad de Cádiz, Apdo. 40, 11510 Puerto Real (Cádiz), Spain*
[c]*Unidad Asociada de Oceanografía Interdisciplinar UCA–CSIC, Universidad de Cádiz, Apdo. 40, 11510 Puerto Real (Cádiz), Spain*

Received 14 January 2004; received in revised form 14 September 2004; accepted 21 September 2004
Available online 28 January 2005

Abstract

The formulation of weak wind-wave/low-frequency current interaction is discussed comprehensively as applied to fixed- and moveable-bottom cases. It involves (1) a dependence of the drag coefficient on the ratio between wave and current bottom friction velocity amplitudes, (2) the resistance law for the oscillatory, rough, turbulent bottom boundary layer (BBL) which accounts for the usually neglected effects of rotation and the phase difference between the bottom stress and the friction-free current velocity, (3) the expression for the BBL depth in terms of the bottom Rossby number and (4) the bottom roughness predictor of Grant and Madsen (J. Geophys. Res., 87 (1982) 469) in the version of Tolman (J. Phys. Oceanogr., 24 (1994) 994). The formulation is implemented in the UCA (University of Cadiz) 2D nonlinear, high-resolution, hydrodynamic model and used to study the influence of wind-wave/tide interaction, bottom mobility and the improved flow-resistance description on the M_2 tidal dynamics of Cadiz Bay. The inclusion of either of the first two factors can cause the drag coefficient to increase significantly over its reference value. If the third factor is included, changes in the drag coefficient are quite moderate. This is because the effect of rotation is opposite in sign to the effect of phase difference, so that these effects taken together very nearly balance. The reason why bottom mobility has such an important influence on shallow-water tidal dynamics as wind-wave/tide interaction has, is the occurrence of the large irregular variations in the drag coefficient that accompany sediment motion.
© 2005 Elsevier Ltd. All rights reserved.

Keywords: Weak wind-wave-tide interaction; Bottom mobility; Resistance law

1. Introduction

Theoretical and experimental investigations of the interaction between wind waves and low-frequency (in particular, tidal) motions began

*Corresponding author. Tel./fax: +34 956 01 6079.
E-mail addresses: kagan@ioras.nw.ru (B.A. Kagan), oscar.alvarez@uca.es (O. Alvarez).
[1]Also for corrospondance.

0278-4343/$ - see front matter © 2005 Elsevier Ltd. All rights reserved.
doi:10.1016/j.csr.2004.09.021

more than 30 years ago and continues till today. This activity is motivated by a pressing need for reducing uncertainties in predictions of wind waves, tides, wind- and density-driven currents and sediment transport in coastal waters.

Bijker (1967) and Hasselmann and Collins (1968) seem to have been the first to attempt a solution for the problem of wind-wave/low-frequency current interaction. In their pioneering works, they assumed that the interaction between motions with different frequencies might be described by combining velocities in the near-bottom layer, instead of through turbulence of different origin. Subsequent studies generally relied on simplified representations of the vertical eddy viscosity in the oscillatory, rough, turbulent bottom boundary layer (BBL) in combined wave and current flows. In fact, the vertical eddy viscosity was considered to be time-invariant and varied with height above bottom such that the solution of the equations describing the BBL vertical structure was analytically tractable (Lundgren, 1973; Smith, 1977; Grant and Madsen, 1979; Tanaka and Shuto, 1981; Myrhaug, 1984; Christoffersen and Jonsson, 1985; Coffey and Nielsen, 1985). The philosophy underlying the models applied was that they should both provide an adequate description of the BBL and was sufficiently simple to use.

In all analytical models it was necessary to make assumptions about the vertical structure of the combined BBL. Because the characteristic time scale of wind waves is much less than the time scale of low-frequency currents (and, consequently, the wave BBL depth is much less than the current BBL depth), the combined BBL was partioned into wave and current BBLs, with the wave BBL nested within the current BBL. However, in this case the wave bottom stress will be much larger than the current bottom stress provided that the friction-free wave and current velocity amplitudes are of the same order of magnitude. This causes the current bottom stress to be greatly enhanced, and the near-bottom current velocity to be reduced compared with their values for the current alone.

Another approach has been adopted by Davies et al. (1988), Davies (1990), Malarkey and Davies (1998), Kagan and Utkin (2000), Kagan et al. (2001, 2003a, b) and Mellor (2002). Having discarded the above restrictive assumptions used in most of the analytical models and supplemented the equations for the combined BBL by one or other turbulence closure schemes, they numerically solved the problem. The resulting solutions confirmed the occurrence of the wind-wave-induced changes in the current bottom stress and the current velocity.

This finding was also supported for combined wind waves and currents by observational data in both the laboratory (Bijker, 1967; Bakker and van Doorn, 1978; Kemp and Simons, 1982; Simons et al., 1988, 1992; Sleath, 1990; Arnskov et al., 1993; Mathisen and Madsen, 1996a, b) and in the field (Cacchione and Drake, 1982; Grant et al., 1984; Grant and Williams, 1985; Myrhaug et al., 1987; Huntley and Hazen, 1988; Soulsby and Humphrey, 1990; Green et al., 1990; Trowbridge and Agrawal, 1995).

In spite of these significant efforts, the problem cannot be regarded as solved for two reasons. First, the above analytical and numerical models provide qualitatively similar results despite differing from one another in the concept. In this connection we point out that there are two concepts of wind-wave/low-frequency current interaction. One suggests that both wave and current bottom stress oscillations are enhanced owing to their nonlinear interaction, so that the bottom stress in a combined motion differs from the sum of the bottom stresses produced by pure wave and low-frequency components of motion. This concept (which may be referred to as the strong interaction concept) forms the basis for the formulation of wind-wave/low-frequency current interaction proposed by Grant and Madsen (1979). It has found application in studies of tides, wind-driven circulation, storm surges, combined tidal and storm-driven flows and suspended sediment transport (see, e.g., Spaulding and Isaji, 1987; Christoffersen and Jonsson, 1985; Signell et al., 1990; Bender and Wang, 1993; Davies and Lawrence, 1994a, b, 1995; Keen and Glenn, 1995; Tang and Grimshaw, 1996; Lou and Ridd, 1997; Davies and Glorioso, 1999). Meanwhile, reanalysis of existing data (Signell et al., 1990) and evidence from one-equation turbulence models for the

oscillatory, rough, turbulent BBL (Davies et al., 1988; Kagan and Utkin, 2000; Kagan et al., 2001) show that there is neither experimental nor theoretical evidence of a strong impact of low-frequency currents on wind waves even in the "strong interaction" approach, while the effect of wind waves on low-frequency currents can be significant. However if the inclusion of wind-wave/low-frequency current interaction is required solely to modify currents, in particular bottom currents, the lack of the evidence in favour of the strong interaction approach is not a deciding argument against. We note in passing that in this case the term "interaction" is irrelevant, but the latter is already the subject matter of a terminological discussion.

An alternative concept suggests that wind-wave/low-frequency current interaction is weak. It starts from the evident consideration that the interaction between motions with widely different spatial and temporal scales can be weak, even though these motions are in themselves strongly nonlinear. The implication is that the bottom stress oscillations due to wave and low-frequency motions are weakly correlated; hence, their linear superposition provides an adequate description of the overall bottom stress. These suggestions serve as a basis for the formulation of weak wind-wave/low-frequency current interaction developed by the authors (Kagan and Utkin, 2000; Kagan et al., 2001, 2003a, b; Kagan, 2003 a).

Second, the currently available field data relating to the problem of interest are sparse and suffer from uncertainty in measurements. In turn, laboratory data in wave flumes and tunnels are restricted to the wave-dominated cases in which waves and currents are either co-linear or orthogonal. It is therefore not surprising that the apparently dissimilar formulations are satisfactorily consistent with the experimental data obtained from CODE-1 and CODE-2 (Grant et al., 1984; Grant and Williams, 1985), which was specifically designed to verify formulations of wind-wave/low-frequency current interaction.

Our purpose here is to summarize theoretical studies of weak wind-wave/low-frequency current interaction and some basic results of their application. This will provide an understanding, in the context of the weak interaction approach, of the roles of wind-wave/tide interaction, bottom mobility and the improved representation of flow resistance in shallow-water tidal dynamics whose predictions, as well as predictions of wind-wave and sediment transport dynamics, depend crucially on whether or not these factors are adequately described.

2. The formulation

We shall consider the near-bottom log layer in low-frequency flow having a time scale defined as the ratio of the layer depth to the bottom friction velocity amplitude. Because the characteristic depth of this layer and the characteristic bottom friction velocity amplitude are equal to 10 m and $1\,\mathrm{cm\,s^{-1}}$ (Bowden, 1978), the time scale is 15 min. It is much smaller than the period of any one of the low-frequency constituents, implying that the condition of quasi-steadiness is fulfilled, and the vertical distribution of velocity adheres to the law of the wall. The same can be said for the wave near-bottom log layer which depth and time scales are at most 10 cm and 10 s. Evidence from laboratory and field observations (see above) provides support for this conclusion. Further, we shall make use of the fact that the wave BBL depth is much less than the current BBL depth and, following Smith (1977), assume that the vertical eddy viscosity in the wave BBL is the sum of the vertical eddy viscosities, each being determined by the wave or current bottom friction velocity amplitude. Above the wave BBL (but within the current log layer) the eddy viscosity is determined by the current bottom friction velocity amplitude. Moreover, we shall assume that the vertical eddy viscosity in the low-frequency log layer, whose depth is considered to be smaller than a local water depth, is a piecewise linear, continuous function of depth, and the bottom roughness lengths in the wave and current BBLs are different from each other and equal to their reference values appropriate to the fixed-bottom case. These reference values of the wave and current bottom roughness lengths are taken as

constants over the whole region of interest and will be specified below.

It is relevant to note in this connection that (1) the bottom roughness length is determined by the entire spectrum of bottom roughness elements over the area with a linear scale of the order of the near-bottom log layer depth; (2) the wave and current log layer depths differ in magnitude; and (3) the geometric properties (dimension, shape and spacing) of bottom roughness elements are distinct from one another and vary spatially and temporally due to sediment motion. These three circumstances together explain why the wave and current reference bottom roughness lengths are being taken as different from each other. By the way, the fact that the bottom roughness length may be different for the wave and current near-bottom log layers is not surprising. Recall the findings of Smith and McLean (1977) who showed that, depending on whether the height above bottom is smaller or greater than the spatial scales of bedforms, the latter act either as elements of bottom topography or as elements of bottom roughness. Thus in the lowest few centimetres, the bottom roughness length is governed by sand grains; above this, by ripples; and higher up, by dunes. As a result, segmented velocity profiles can occur, but are only seen infrequently.

Then, on defining the drag coefficient in the presence and absence of wind waves (c_D and c_{DO}, respectively) as

$$c_D^{-1/2} = U_{T1}/U_{*T};\;\; c_{DO}^{-1/2} = \kappa^{-1}\ln(z_1/z_{0T}^r) \tag{1}$$

we find from the condition of continuity of velocity at the top of the wave BBL in the fixed-bottom case (Kagan et al., 2001)

$$c_D^{-1/2} = c_{DO}^{-1/2} - \frac{1}{\kappa}\left[\ln(1+\gamma) + \gamma(1+\gamma)^{-1} \times \ln\left(\frac{\delta_w}{z_{0w}^r}\right)\left(\frac{z_{0w}^r}{z_{0T}^r}\right) - \ln\left(1+\gamma\left(\frac{\delta_w}{z_{0w}^r}\right) \times \left(\frac{z_{0w}^r}{z_{0T}^r}\right)\exp\left(-\kappa c_{DO}^{-1/2}\right)\right)\right] \tag{2}$$

where U_{T1} is the wave-affected current velocity amplitude at the height z_1 within the current log layer but above the wave BBL; U_{*T} is the current bottom friction velocity amplitude; z_{0w}^r and z_{0T}^r are the wave and current reference bottom roughness lengths which are defined as fixed-bottom roughness lengths and determined either by the Nikuradse sand grain roughness or by the background bottom roughness of relict origin, and κ is von Karman's constant.

The remaining unknown quantities that appear in Eq. (2)—the interaction parameter, γ, representing the ratio between the wave and current bottom friction velocity amplitudes and the scaled wave and current BBL depths, δ_w/z_{0w}^r and δ_T/z_{0T}^r (here, δ_w and δ_T are the wave and current BBL depths, the latter will be needed later)—are defined as

$$\gamma = \sqrt{\frac{f_w}{f_T}}\frac{U_{w\infty}}{U_{T\infty}}, \tag{3}$$

$$\frac{\delta_w}{z_{0w}^r} = \kappa\sqrt{\frac{f_w}{2}}Ro_w,\;\; \frac{\delta_T}{z_{0T}^r} = \kappa\sqrt{\frac{f_T}{2}}Ro_T\left(1+\frac{f}{\sigma_T}\right)^{-1}, \tag{4}$$

where $f_w = 2(U_{*w}/U_{w\infty})^2$ and $f_T = 2(U_{*T}/U_{T\infty})^2$ are the wave and current bottom friction factors, U_{*w} is the wave bottom friction velocity amplitude, $U_{w\infty}$ and $U_{T\infty}$ are the wave and current friction-free velocity amplitudes, $Ro_w = U_{w\infty}/\sigma_w z_{0w}^r$ and $Ro_T = U_{T\infty}/\sigma_T z_{0T}^r$ are the wave and current bottom Rossby numbers, σ_w and σ_T are wave and low frequencies, and f is the inertial frequency.

The wave and current bottom friction factors are inferred, with allowance made for weak correlation between the wave and current bottom stresses, from the resistance law for the oscillatory, rough, turbulent BBL. Including the usually neglected effects of rotation and the phase difference between the bottom stress and the friction-free current velocity, this resistance law becomes (Kagan, 2003b)

$$\left[(2,3A)^2 + \left(2,3B + \ln 2^{-5/2}\kappa + \frac{2^{5/2}\kappa}{4\sqrt{f_w}}\right)^2\right]^{1/2} = \ln 2^{-5/2}\kappa - \ln\frac{1}{4\sqrt{f_w}} + \ln Ro_w, \tag{5}$$

for the wave BBL and

$$\left[(2,3A)^2+\left(2,3B+\ln 2^{-5/2}\kappa+\sqrt{\left(\frac{2^{5/2}\kappa}{4\sqrt{f_T}}\right)^2-(2,3C)^2}\right)^2\right]^{\frac{1}{2}}=\begin{cases}\ln 2^{-5/2}\kappa-\ln\frac{1}{4\sqrt{f_T}}-\ln\left(1+\frac{f}{\sigma_T}\right)+\ln Ro_T & \text{if } \delta_T<h,\\ \ln\frac{h}{z_{0T}^r}, & \text{if } \delta_T\geqslant h,\end{cases}\tag{6}$$

for the current BBL. Here, h is the local water depth, and A, B and C are numerical constants derived from laboratory and field observations and equal to 0.92, 1.38 and 2.17, respectively. It should be stressed that Eqs. (5) and (6) were obtained without specifying a certain vertical eddy viscosity profile outside the near-bottom log layer. These were derived by matching the asymptotic expressions for velocity in the near-bottom log layer and the outer part of the BBL at intermediate depths (in the overlapping range where both these expressions are simultaneously valid). For detailed derivation of Eqs. (5) and (6) see Kagan (2003b).

The set of Eqs. (2)–(6) determines uniquely the drag coefficient, c_D, in a wave-affected, low-frequency flow, provided that, for a given c_{D0}, the following dimensionless parameters are specified: the ratio between the wave and current friction-free velocity amplitudes, $U_{w\infty}/U_{T\infty}$, the wave and current bottom Rossby numbers, Ro_w and Ro_T (the latter is replaced by the ratio of the local water depth to the current reference bottom roughness length, h/z_{0T}^r, if the current BBL extends to the sea surface), the ratio between the wave and current reference bottom roughness lengths, z_{0w}^r/z_{0T}^r, and the ratio between the inertial and low frequencies, f/σ_T. We stress once more that the wave and current reference bottom roughness lengths are not generally the same and that the use of a single time-invariant reference bottom roughness length is an assumption which should be justified in each specific case.

To estimate sediment-motion-induced changes in low-frequency flow dynamics, we shall extend the formulation of weak wind-wave/low-frequency current interaction to the moveable-bottom case. For this purpose, we adopt the popular (in the wave community) bottom roughness predictor of Grant and Madsen (1982) as modified by Tolman (1994). Following Tolman (1994), we suggest that the bottom roughness is in one of three regimes, depending on the value of the Shields parameter (the ratio of the driving drag force acting on a sediment particle to the retarding buoyancy force). The first occurs when forcing is too weak to initiate sediment motion and the bottom roughness is taken as the reference roughness determined by the relict bottom roughness. As the Shields parameter increases to the critical value for initial sediment motion, ripples begin to form. Accordingly, the bottom roughness increases by a jump to the ripple roughness. As the Shields parameter increases further, ripples reach an equilibrium state and then are gradually smoothed out, which decreases the bottom roughness. The smoothing-out process is accompanied by the development of a sheet flow (the flow of highly concentrated rolling, saltating, and suspended sediment particles) in the near-bottom layer, and the bottom roughness is identified with the sheet-flow roughness. In the general case, which encompasses all sediment motion regimes, the bottom roughness is obtained by matching of the appropriate asymptotes. It is this expression for the bottom roughness length that serves as the bottom roughness predictor. In the case being discussed, the weak interaction between wind waves and low-frequency currents is described by the same Eqs. (2)–(6), with the only difference being that the expression for the drag coefficient is now rewritten as (see Kagan et al., 2003a)

$$c_D^{-1/2}=c_{DO}^{-1/2}-\frac{1}{\kappa}\left[\ln(1+\gamma)+\gamma(1+\gamma)^{-1}\ln\left(\frac{\delta_w}{z_{0w}^r}\right)\times\left(\frac{z_{0w}^r}{z_{0T}^r}\right)+(1+\gamma)^{-1}\ln\left(1+m\frac{z_{0w}^r}{z_{0T}^r}\right)-\ln\left(1+\gamma\left(\frac{\delta_w}{z_{0w}^r}\right)\left(\frac{z_{0w}^r}{z_{0T}^r}\right)\exp\left(-\kappa c_{DO}^{-1/2}\right)\right)\right],\tag{7}$$

where m is the mobility parameter defined as the ratio between sediment motion-induced changes in the bottom roughness length to its reference value.

We shall refer to the process of changing the bottom roughness as "bottom mobility" and take the bottom roughness length as the sum of its

reference value and sediment motion-induced changes. Then, considering that the wave bottom stress is much larger than the current bottom stress, the sediment-motion-induced changes in the bottom roughness length may be expected to be of wave origin. However, if the wave and current reference bottom roughness lengths are different in magnitude, and the time scale of the ripple generation is much less than the time scale of the wave-field evolution, which suggests a jump-like change in the bottom roughness, the wave and current bottom roughness lengths (z_{ow} and z_{oT}, respectively) are

$$z_{0w} = z^r_{0w}(1+m),\quad z_{0T} = z^r_{0T}\left(1 + m\frac{z^r_{0w}}{z^r_{0T}}\right), \tag{8}$$

where, according to Tolman (1994),

$$m = \begin{cases} 0 & \text{if } \theta'/\theta' < 1,2, \\ 0.05 Ro_w \left(\frac{\theta'}{\theta'_c}\right)^{-2,5} + 0.218\times 10^{-2} Ro_w^{2,4}\left(\sigma_w\sqrt{\frac{d}{g'}}\right)^{2,8}\left(\frac{d}{z^r_{ow}}\right)^{-1,4} & \text{if } \theta'/\theta' \geqslant 1,2, \end{cases} \tag{9}$$

θ' is the skin friction Shields parameter specified in terms of Ro_w as

$$\theta' = \frac{f'_w}{2} Ro'^2_w \left(\sigma_w\sqrt{\frac{d}{g'}}\right)^2 \left(\frac{d}{z^r_{0w}}\right)^{-2}, \tag{10}$$

Ro'_w is the wave bottom Rossby number based on z_0', f_w' is the skin friction factor defined as $f'_w = f_w$ at $z_{0w} = z'_0$, $z'_0 = d/30$ is the sediment grain roughness length, d is the mean grain size, θ'_c is the critical Shields parameter for the initiation of sediment motion, $g' = g(\rho_s - \rho_w)/\rho_w$ is reduced gravity, g is the acceleration due to gravity, and ρ_s and ρ_w are sediment and sea water densities, respectively.

Notice that in shallow, tide-dominant basins where sediment motion can be caused by both wind waves and tides, the right-hand side of Eq. (10) must be multiplied by the factor $\left(1+\gamma'^2\right)/\gamma'^2$, which characterizes the contribution of tides to the overall skin friction. Here, $\gamma' = \gamma$ at $z_{0w} = z_{0T} = z'_0$. Of course, wind-driven currents can also transport sediment. However this is another problem which is not considered in the present paper.

From Eqs. (2) to (10) it follows that, if wind-wave/low-frequency current interaction and bottom mobility are concurrently accounted for, the drag coefficient is determined by seven (not five as in the fixed-bottom case) dimensionless parameters, namely $U_{w\infty}/U_{T\infty}$, Ro_w, Ro_T, z^r_{0w}/z^r_{0T}, f/σ_T, $\sigma_w(d/g')^{1/2}$ and d/z^r_{0w}. Here, $\sigma_w(d/g')^{1/2}$ is the ratio of the representative wave frequency, σ_w, to the buoyancy frequency, $(g'/d)^{1/2}$, of suspended sediment particles; the remaining designations have already been defined.

In a sensitivity study with these parameters Kagan (2003a) shows that changes in c_D over ranges of typical values of Ro_w, $\sigma_w(d/g')^{1/2}$ and $d/z^r{}_{0w}$ are not too large, while in the ranges of typical values of $U_{w\infty}/U_{T\infty}$, Ro_T and z^r_{0w}/z^r_{0T} they may amount to as much as two-three orders of magnitude. The strong sensitivity of the drag coefficient to variations in $U_{w\infty}/U_{T\infty}$, Ro_T and z^r_{0w}/z^r_{0T} imposes rigorous requirements on the accuracy of evaluating these parameters in field conditions. In this connection it should be remembered that if $U_{w\infty}/U_{T\infty}$ and Ro_T are determined from observational data with some degree of certainty, then z^r_{0w}/z^r_{0T} can only be estimated by informed guessing.

3. The investigation site and the model

The above formulation of wind-wave/low-frequency current interaction has been adopted to clarify the roles of wind-wave/tide interaction, bottom mobility and the improved flow-resistance representation in shallow-water tidal dynamics. Cadiz Bay is chosen as an investigation site where detailed tide-gauge and bottom pressure measurements have been made during the last few years.

Cadiz Bay is near 36.5° N latitude on the south-west coast of Spain. It faces west toward the Gulf of Cadiz and is landlocked around its

south-western, southern and eastern margins by the mainland. The bay is subdivided into two parts, the shallower Inner Bay and deeper Outer Bay, connected by narrow Puntales Channel (Fig. 1). The bay is shallow, with a maximum depth of 20 m at its seaward edge, and is characterized by predominantly semi-diurnal co-oscillating tides with an amplitude of ~1 m for the M_2 constituent. The typical wind waves in Cadiz Bay are short-period waves whose spectrum is similar to that in finite-depth water. It is marked by a rather sharp peak and a high-frequency flank that follows a -3.5 power law. On the low-frequency flank there is a second peak at the swell frequency. Swell periods are 12–15 s. An rms wave amplitude and a spectrally averaged wave period corresponding to this "climatologic" wave spectrum in spring are 0.67 m and 5.7 s, respectively. It is these wave parameters that were applied to evaluate the near-bottom, friction-free, wave orbital velocity amplitudes. Sea-bed sediments in the bay consist mainly of coarse silt with a median grain size of ~40 μm and medium sand with a median grain size of ~190 μm. Quartz grains comprise 85% of all sediments (Gutierrez et al. (1996)).

The UCA 2D nonlinear, high-resolution, hydrodynamic model developed by Alvarez et al. (1997) has been applied to simulate the M_2 tidal dynamics of Cadiz Bay. The model is based on the mass-conservation and momentum equations in depth-averaged form. A condition of no-flow normal to the coast is set at the land boundaries. Since the simulation of high-precision fields of tidal characteristics is not the prime focus of this paper, the effects of flooding and drying of mud flats are not considered despite the fact that these may be important in shallow, tide-dominant basins. Instead, the land boundaries are vertical walls at the local water depth of 1 m. At the open boundary, a radiation condition, written in terms of deviations of tidal elevation and velocity from their observed values, is employed to ensure that, when numerical disturbances are generated, they all propagate away from the model domain. The observed values of tidal elevation along the open boundary are obtained using a linear interpolation/extrapolation of those derived from the bottom pressure

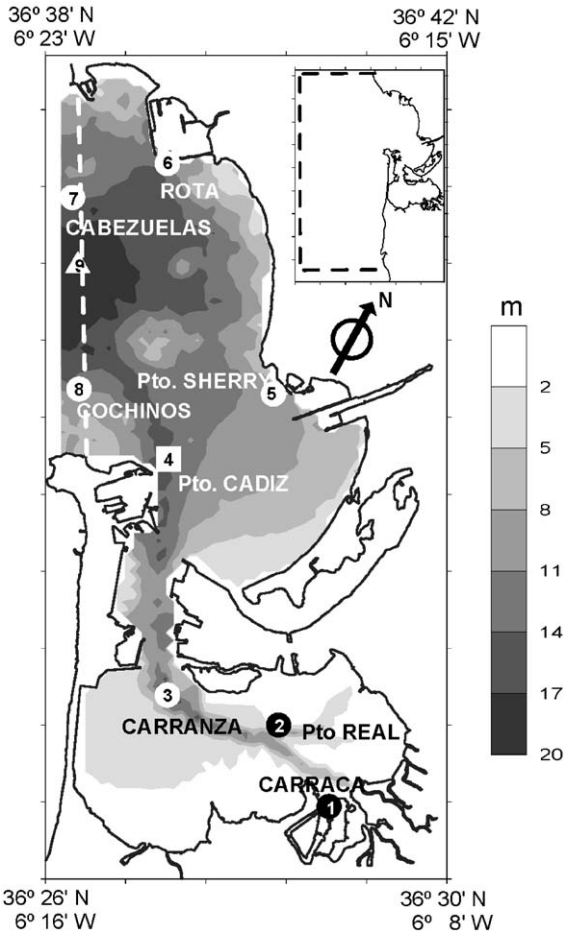

Fig. 1. Map of Cádiz Bay superimposed on the bathymetry (in m). The location of a tide-gauge is denoted by the square, the locations of the bottom-pressure sensors, by open and closed circles; and the location of a current-mooring, by the triangle. An extended domain is shown in the inset. Dotted lines denote the open boundaries of Cádiz Bay and the extended domain.

measurements at stations Cochinos and Bajo de Cabezuelas, while the observed values of tidal velocity are taken as being equal to the M_2 tidal velocity derived from the data at the current-meter mooring location at the open boundary.

The above radiation condition is set at the entrance to the bay only in the case when all the factors we are interested in are taken into account (this case most closely corresponds to real conditions). In the other cases when any of these factors is ignored, the observed tidal characteristics at the

entrance cannot be obtained in the same manner because the observations are subjected to the influence of within-bay processes and do not remain unaltered under different conditions. In these cases to minimize the influence of the internal hydrodynamics of the bay on tidal elevation and velocity at the entrance, the computational domain extends into the adjacent Gulf of Cadiz to depths of 50 m and more, so that the open boundary of the extended domain (see the inset in Fig. 1) was out of the domain of influence of Cádiz Bay. The observed tidal elevations and velocities along this boundary are those computed from Tejedor et al.'s (1998) tidal model. For the solution to be smooth the equations of motion are supplemented by a Laplacian horizontal eddy diffusion operator acting on the tidal velocity throughout the model domain except along the boundaries. The horizontal eddy viscosity is kept, for purely computational considerations, to a minimum of $1\,m^2s^{-1}$ to suppress short-wavelength numerical disturbances but, at the same time, to avoid excessively strong smoothing of the derived solution.

The bottom stress related to the depth-averaged tidal velocity is parameterized by a quadratic resistance law with the drag coefficient taken as previously described in order to account for the influence of the factors considered. The reference drag coefficient and the wave and tidal reference bottom roughness lengths are set to be $c_{DO} = 0.003$, $z^r_{0w} = 0.03$ cm and $z^r_{0T} = 0.5$ cm. The first of these reference bottom roughness lengths is specified as accepted by Tolman (1994), and the second, as being approximately appropriate to the prescribed value of c_{DO}. As noted by Heathershaw (1981), c_{DO} and z^r_{0T} do not remain constant if there are changes in bed type and sediment grain size. The assumption of constancy of these quantities, however, is probably reasonable for Cadiz Bay where no significant spatial variations in bed types and forms occur. For a detailed discussion of this subject see Aldridge and Davies (1993) and Davies and Lawrence (1995).

In this paper, the wave friction-free velocity amplitude is calculated from linear wave theory using known values of wave amplitude, wave frequency and local water depth. Throughout the bay, except for the near-shore shallows, the wave amplitude and frequency are identified, respectively, with the rms amplitude and the spectrally averaged wave frequency derived from the typical (''climatological'') wave spectrum and local water depth. In the shallows, where depths are less than twice the wave amplitude, the latter is assumed to be depth-limited due to wave breaking and equal to half of the local water depth. This condition is equivalent to the empirical wave-breaking criterion employed by Tang and Grimshaw (1996). Of course, the ''climatological'' wave spectrum, which, in addition, is based upon measurements at the open boundary of the bay and is not modified for appropriate within-bay conditions, is of limited application, but a discussion of this point is beyond the scope of our paper.

As an approximate estimate (which falls in the range of the observed values), the mean grain size is prescribed to be 50 μm. Sensitivity results of varying the mean grain size in the no-wave case have been presented in Alvarez et al. (1999). The critical Shields parameter, reduced gravity and von Karman's constant are set to be 0.05, $1.65 \times 10^3\,cm\,s^{-2}$ and 0.4, respectively. The bathymetry is digitized from the IHM chart number 443.

The model equations are integrated on an Arakawa C staggered grid, using a semi-implicit Crank–Nicolson scheme. A spatial resolution of 210 m and time step of 30 s are chosen. The model is run for 10 tidal cycles to achieve a stable time-periodic solution. After establishing this solution, the model run is continued for one more tidal period so as to determine the M_2 tidal elevation and velocity constants through a harmonic analysis of the relevant time series. Thereafter the cotidal chart and the maps of tidal velocity ellipse parameters and mean (over a tidal cycle) tidal energy budget characteristics are constructed.

4. Results

We shall discuss basic results of four numerical experiments performed using the above-modified model. Experiment 1 corresponds to a conventional approach in which the drag coefficient is considered constant and equal to its reference

value throughout the bay. Experiment 2 includes the effects of wind-wave/tide interaction and ignores all the other effects considered here. The last assumption is equivalent simply to setting zero values of m, f, C and A in Eqs. (2)–(10). In Experiment 3, allowance is additionally made for the usually neglected effects of rotation and phase difference in the resistance law, whereas the effects of bottom mobility are disregarded ($m = 0$) as before. Finally in Experiment 4, the effects of bottom mobility are accounted for.

The model results are displayed in Figs. 2–8. The drag coefficient in Experiment 1 is not illustrated because it is everywhere 3×10^{-3}. As expected, the drag coefficient in the wave-affected tidal flow (Experiment 2) increases throughout the bay (Fig. 2a); the most dramatic changes are eight-fold greater than the no-wave case (Experiment 1) in the shallow Inner Bay. These changes are followed by enhanced bottom stress (Fig. 3b). Maximum changes in the bottom stress occur in regions of strong tidal currents, especially in the Puntales Channel and the shallows. There, the maximum bottom stresses are about 1.5 times greater than those in Experiment 1. The enhanced bottom stresses tend to decrease the tidal velocities in these regions (Fig. 4b). The maximum depth-averaged tidal velocities are reduced by 4–8 cm s^{-1} in the Puntales Channel and 2–4 cm s^{-1} in the shallows. Similar changes in these tidal characteristics have been detected in the eastern Irish Sea as well (Davies and Lawrence, 1994a). As found here, c_D increased by more than a factor of five and resulted in a substantial decrease in tidal velocity. In contrast, the resulting bottom stress was close to that predicted in the no-wave case.

Another interesting point is that the enhanced bottom stress is accompanied by an increase of the maximum depth-averaged tidal velocities in the deeper regions of the Outer Bay. This is due to an enhancement of the mean influx of tidal energy from the Gulf of Cadiz into the Cadiz Bay (Kagan et al., 2001). Because in small basins, such as Cadiz Bay, the mean influx of tidal energy from adjacent basins is balanced by the integral (over the basin considered) mean tidal energy dissipation, the wave-enhanced mean tidal energy influx must therefore increase the mean tidal energy

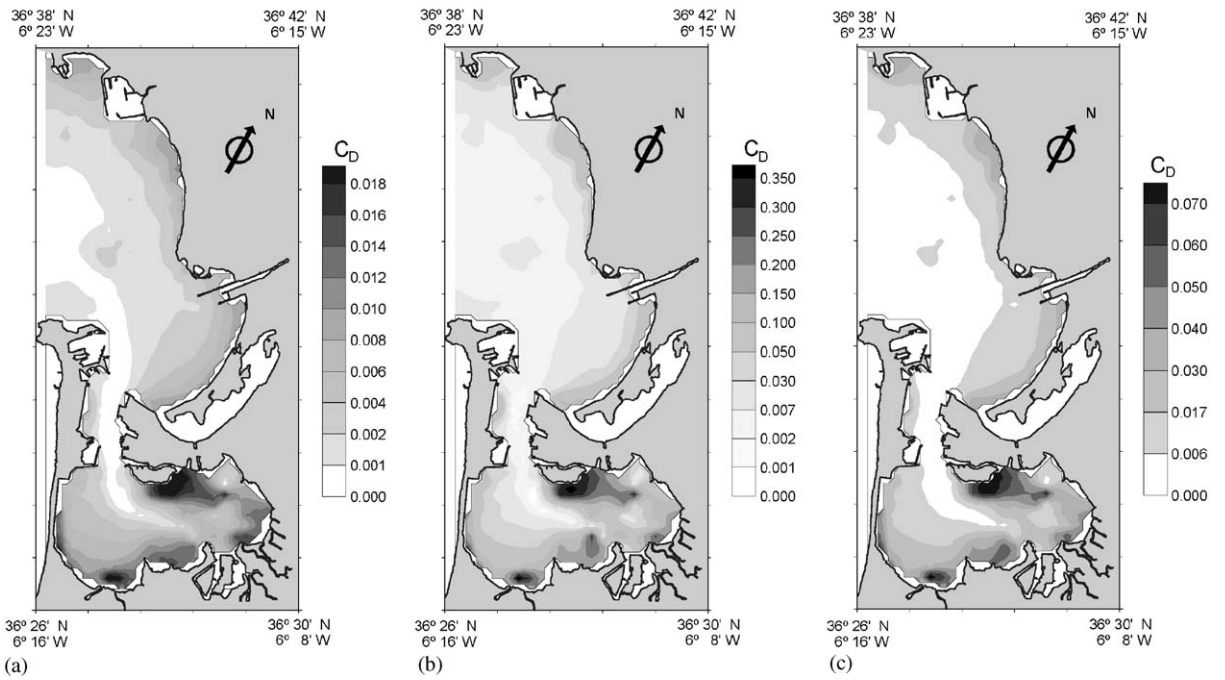

Fig. 2. Changes in the drag coefficient relative its values in Experiment 1 as derived in Experiments 2–4 (panels a–c, respectively).

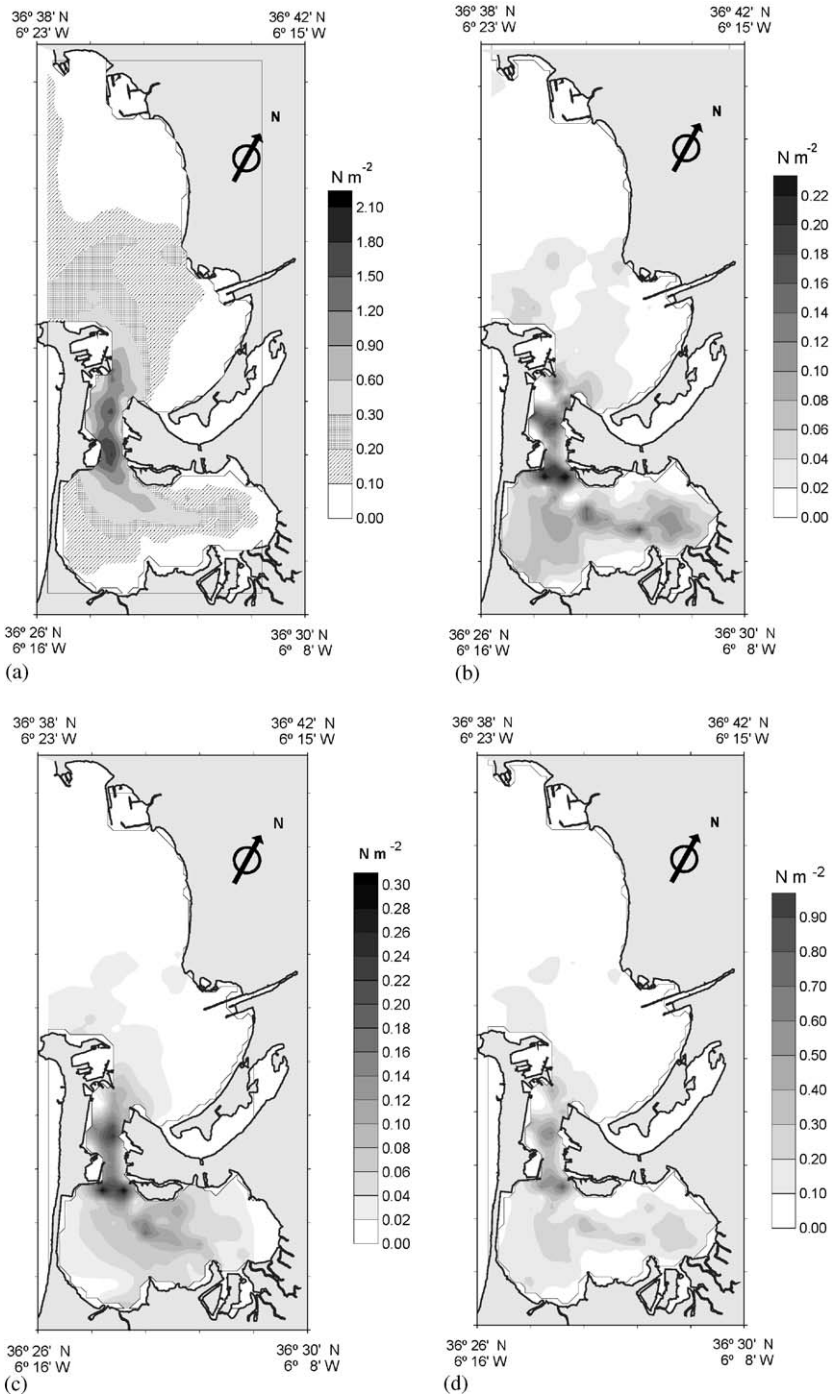

Fig. 3. Maximum bottom stress predicted in Experiment 1 (a) and its changes as derived in Experiments 2–4 (panels b–d, respectively).

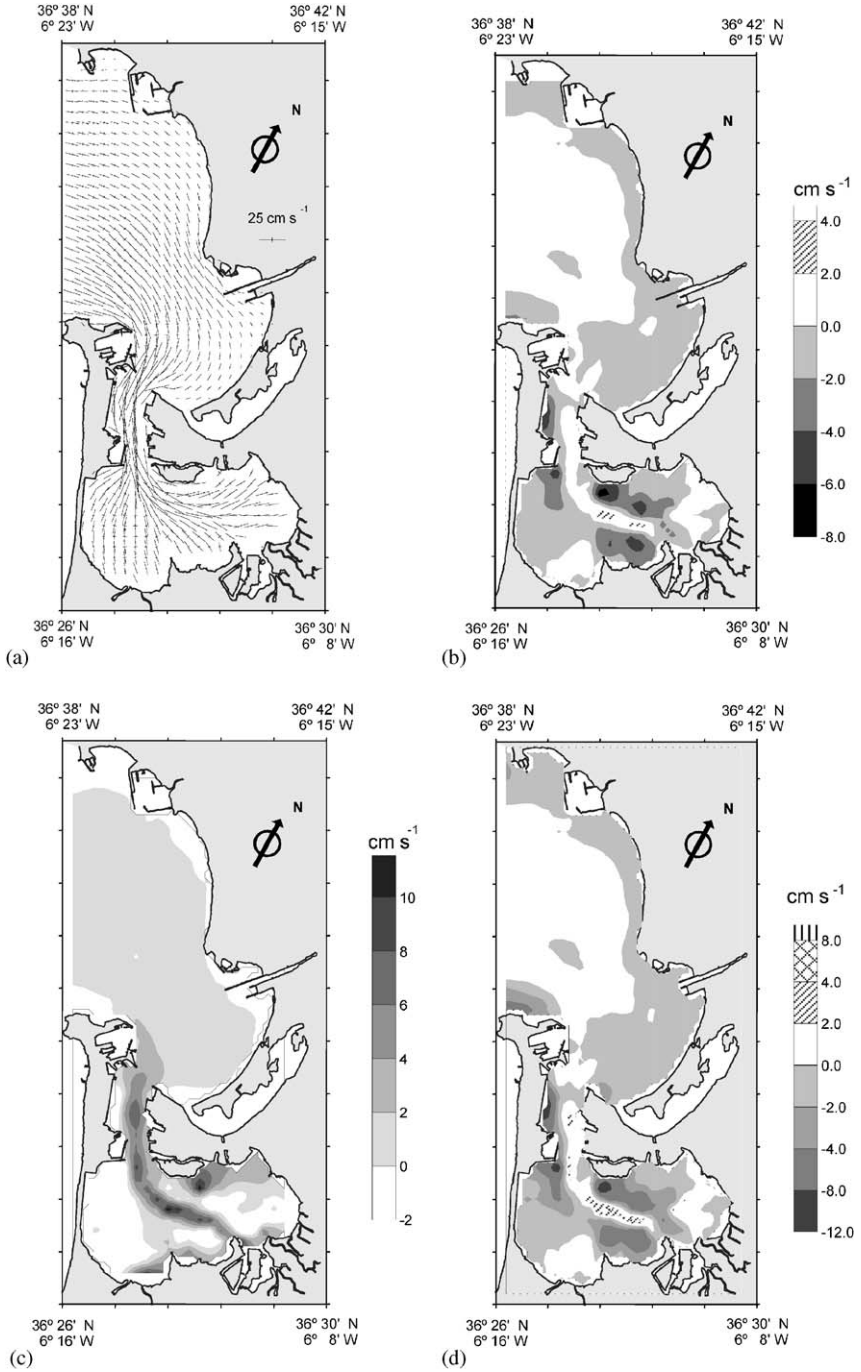

Fig. 4. The same as in Fig. 3 for major and minor axes of the M_2 tidal ellipses.

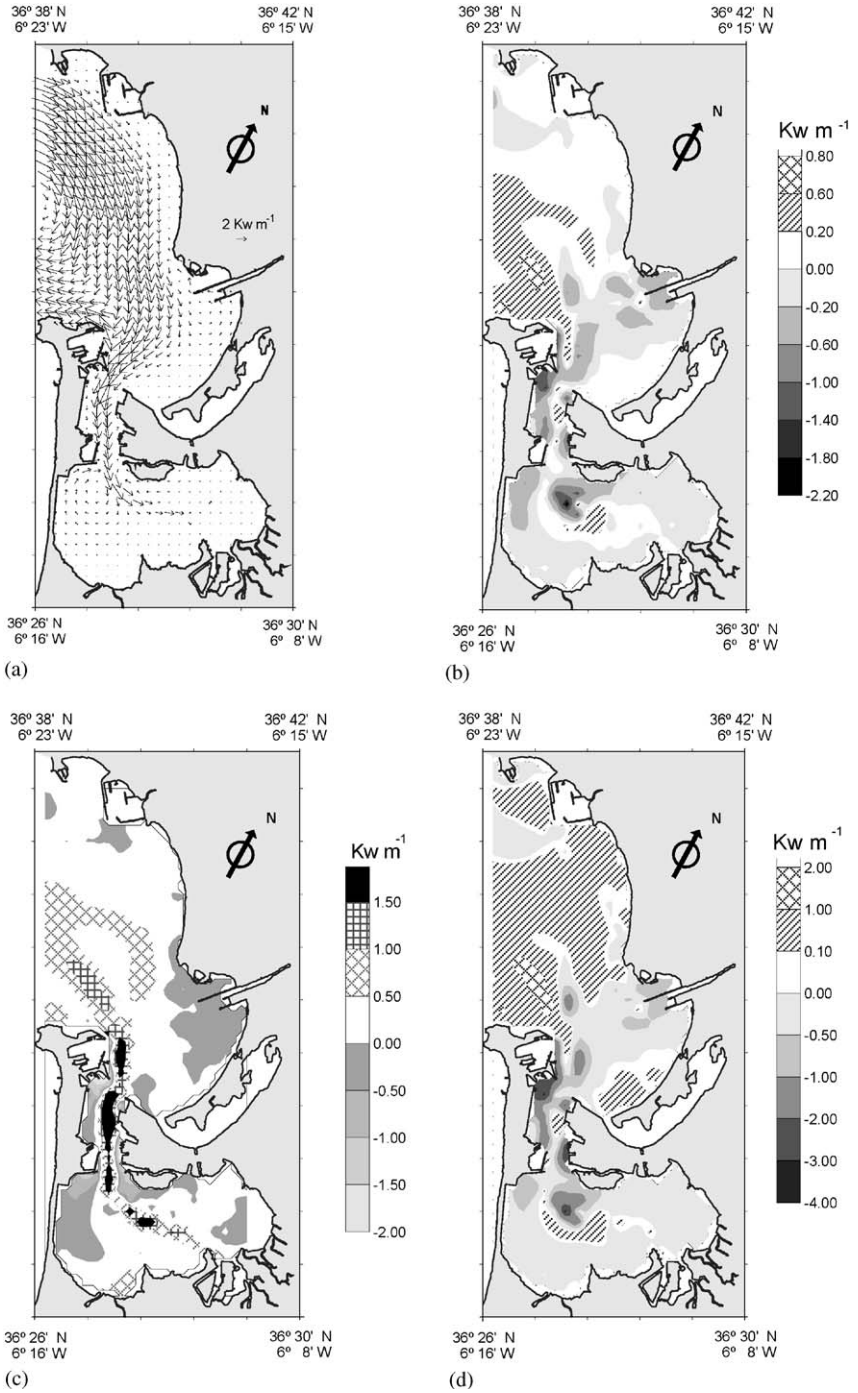

Fig. 5. The same as in Fig. 3 for the mean tidal energy flux per unit length.

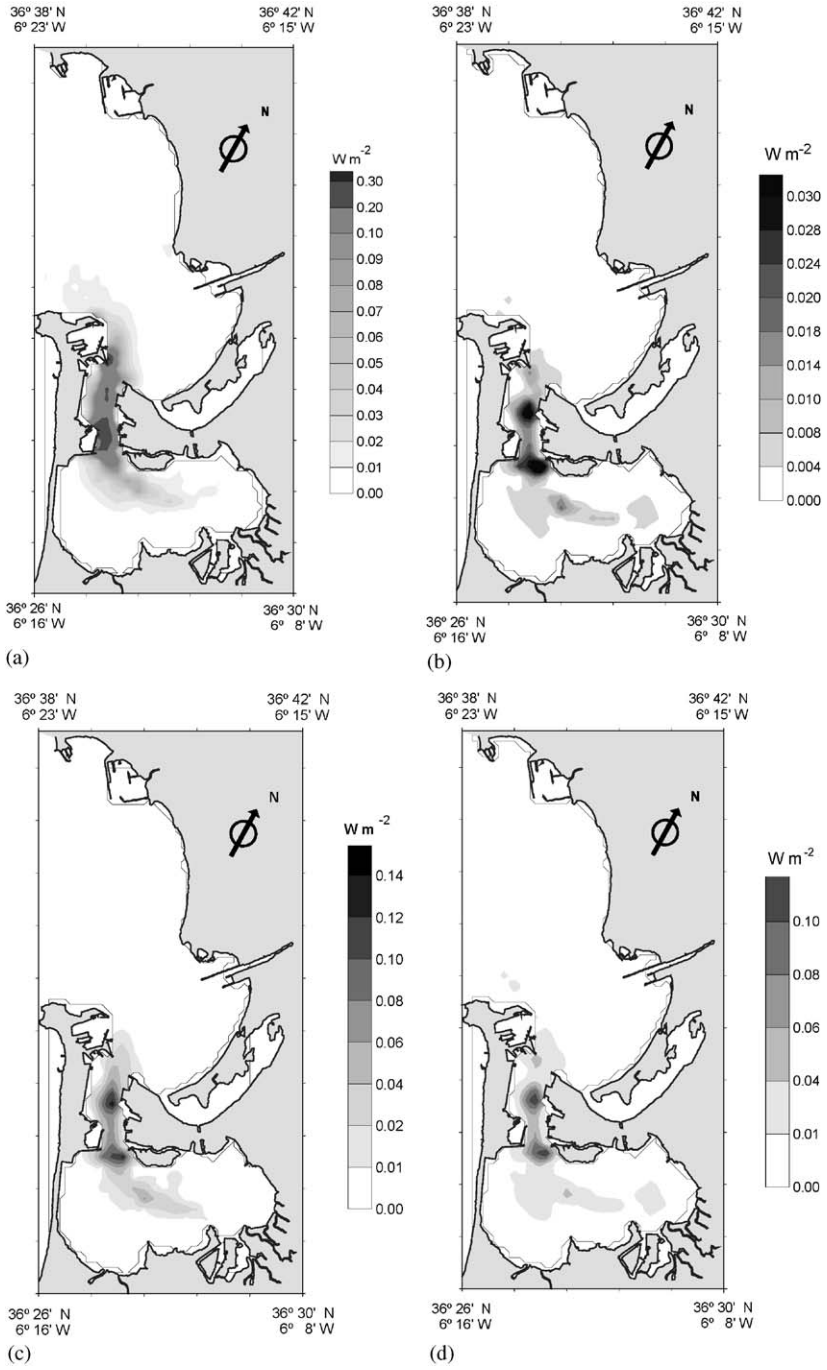

Fig. 6. The same as in Fig. 3 for the mean tidal energy dissipation.

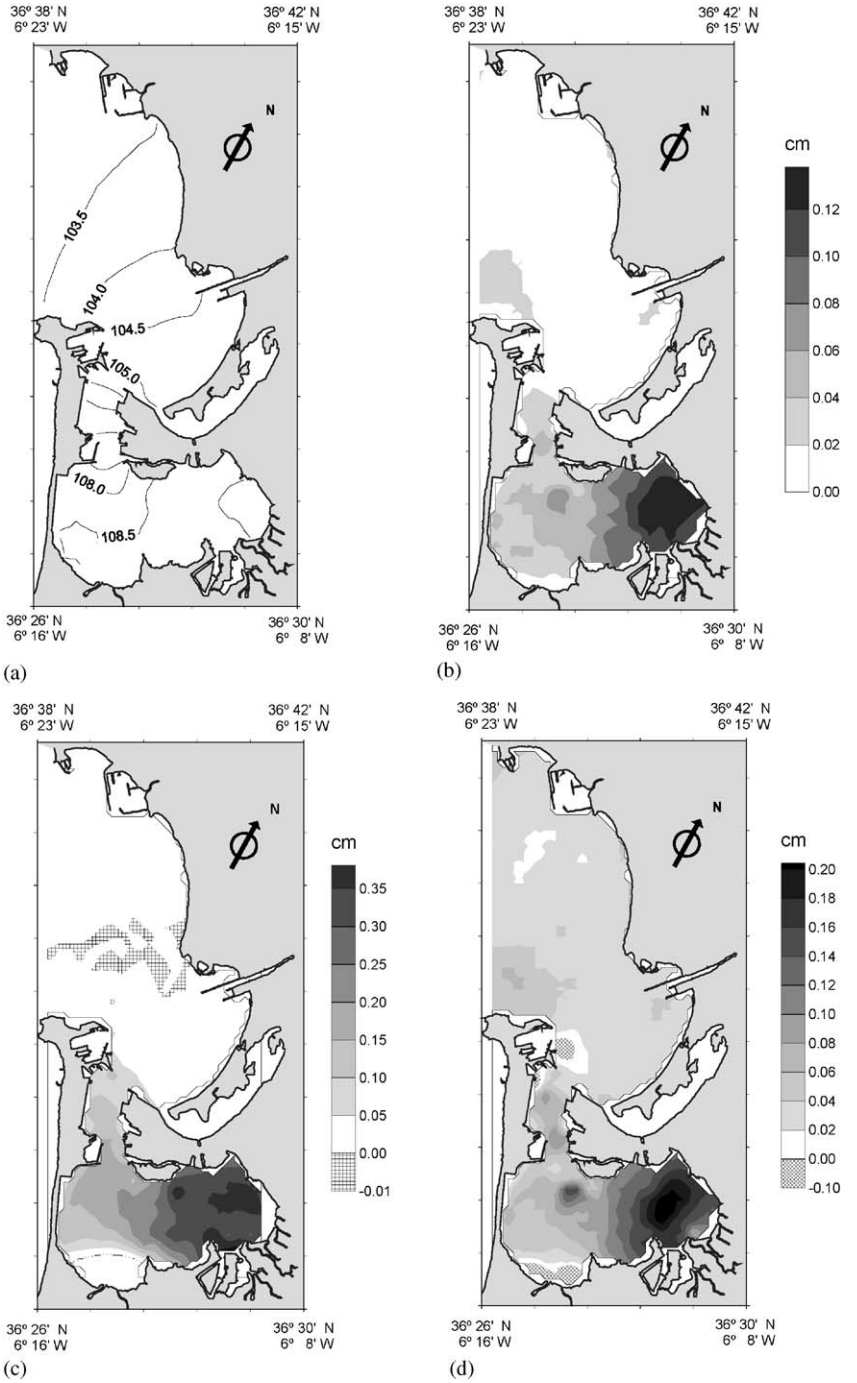

Fig. 7. The same as in Fig. 3. for the tidal elevation amplitude (cm).

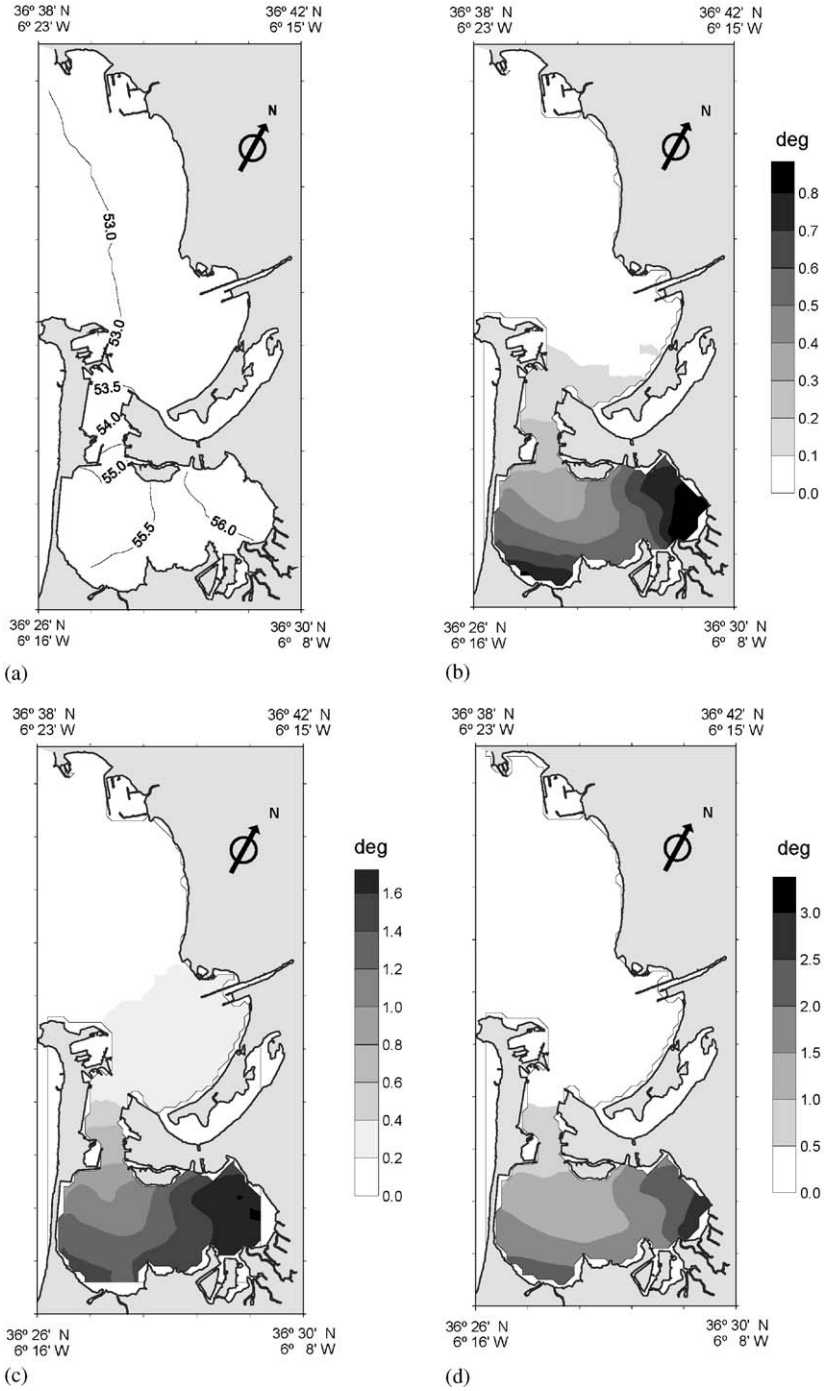

Fig. 8. The same as in Fig. 3 for the tidal elevation phase (deg).

dissipation in the Cadiz Bay. These features are apparent in Figs. 5b and 6b.

As expected the wave-enhanced bottom stress tends to decrease the tidal elevation amplitude and increase the tidal elevation phase throughout the bay (Figs. 7b and 8b). The maximum changes in these characteristics are found in the shallow Inner Bay, but even there these changes do not lead to a radical alteration in the M_2 tide spatial structure. We emphasize once more that these results were obtained using the "climatological" wave spectrum with the above-mentioned rms amplitude and spectrally averaged wave period and that the latter were considered to be invariant throughout the bay excluding its near-shore shallows. Clearly, the results at issue can serve only as illustration.

Including rotation and the phase difference between the bottom stress and the friction-free tidal velocity in the resistance law (Experiment 3) tends to increase the drag coefficient and the tidal elevation phase and decrease the tidal velocity and the tidal elevation amplitude. However, the relative changes in these tidal characteristics are quite moderate and do not exceed 15% (Figs. 2c–8c). Rotation and the phase difference only slightly affect tidal dynamics because these factors cause opposing changes in the tidal bottom friction velocity amplitude. Consequently, their individual effects are partially offset, so that tidal characteristics are similar to those of Experiment 2.

Before describing the next experiment, note that wind-wave/tide interaction and bottom mobility set up qualitatively similar changes in tidal characteristics. The reason is that, according to the bottom roughness predictor used, sediment motion, whether in the ripple or sheet-flow regime, gives rise to increasing bottom roughness length. Thus, both of factors increase the drag coefficient, causing the drag coefficient to exceed 0.070—nearly four times greater than in Experiment 2 (Fig. 2c). As in Experiment 2, the drag coefficient reaches its maximum at the periphery of the Inner Bay where it is 0.069, while in the Puntales Channel and the Outer Bay it is everywhere (except for the shallows) smaller than 0.005. Accordingly, the tidal characteristics from Experiment 4 differ slightly from those predicted in Experiment 2 as shown in Table 1 and Figs. 3d–8d.

Interestingly, bottom mobility has as important influence on tidal dynamics as the interaction between wind waves and tides. This is caused by large irregular variations in the drag coefficient that accompany sediment motion. As evident from the comparison in Table 2, the inclusion of wind-wave/tide interaction, bottom mobility and the improved flow-resistance representation provides a slightly better agreement between the predicted and observed tidal elevation amplitudes and phases than predictions obtained without accounting for these factors. Unfortunately, the lack of observational data confines a quantitative assessment of model performance only by comparing the tidal elevation amplitudes and phases. Using these as the base, the appropriate differences between the observed and predicted tidal characteristics can readily be calculated.

It should be borne in mind, however, that changes in the M_2 tidal elevation amplitudes and phases are not the best indicators of the variations caused by the factors under consideration. This is because, first, the tidal elevation amplitudes and phases characterize only an integral and not a local (especially, in the near-bottom layer) response of the bay to changes due to these factors. Second, the M_2 tide as the dominant one in Cádiz Bay (Álvarez, 1999) is less sensitive to the impact of one factor or the other than other tidal constituents. This explains why the predicted values in Experiments 2–4 are slightly better agree with the

Table 1
Maximum (within the bay) values of tidal characteristics predicted in Experiments 2 and 4

Characteristic	Experiment 2	Experiment 4
Bottom stress (Nm^{-2})	1.4	1.7
Maximum depth—averaged tidal velocity (cms^{-1})	50.0	51.0
Mean tidal energy flux per unit length (Kwm^{-1})	9.0	8.3
Tidal elevation amplitude (cm)	109.1	108.8
Tidal elevation phase (deg)	57.2	57.7
Mean tidal energy dissipation (Wm^{-2})	0.24	0.27

Table 2
Comparison between observed and predicted tidal elevation amplitude A and phases φ

No	Station	Observed		Predicted							
		A(cm)	φ (deg)	Experiment 1		Experiment 2		Experiment 3		Experiment 4	
				A(cm)	φ (deg)	A(cm)	φ (deg)	A(cm)	φ (deg)	A(cm)	φ (deg)
1	Carraca	108.0	60.0	109.2	56.3	109.1	56.9	108.7	56.3	108.8	57.5
2	Pto. Real	106.5	57.9	109.0	56.6	108.4	57.2	108.1	56.6	108.6	57.7
3	P. Carranza	107.2	57.7	107.3	55.2	107.3	55.5	106.8	55.2	107.3	56.3
4	Pto. Cadiz	103.1	55.0	104.6	53.0	103.1	53.0	104.1	53.0	103.1	53.2
5	Pto. Sherry	103.2	52.6	104.0	53.2	103.2	53.2	103.5	53.2	103.2	53.3
6	Rota	101.4	53.8	103.3	53.1	101.4	53.1	102.8	53.1	101.4	53.2

Note: Observations within Cádiz Bay (their locations are shown in Fig. 1) are taken from Alvarez, (1999). Here, too a proof of the validity of observed estimates presented in Table 2 was provided. It was obtained by comparing tidal constants resulting from monthly and yearly time series of sea level elevation.

observations than in Experiment 1. If so, it would seem that a better insight into the nature of the problem being discussed could be given through the study of not the M_2 tide but its higher harmonics (the M_4 and M_6 overtides) caused by energy transfer from the principal tidal constituent primarily via nonlinear bottom friction. Since wind-wave/tide interaction is responsible for significant changes in bottom friction, significant changes would show up in the amplitudes and phases of these overtides as well. That such is indeed the case has been revealed in Kagan et al. (2003b).

5. Summary and conclusions

The formulation of weak wind-wave/low-frequency current interaction has been discussed comprehensively as applied to the fixed- and moveable-bottom cases. The interaction is parameterised in terms of the drag coefficient, an input parameter in any 2D or 3D hydrodynamic models. The bottom roughness predictor of Grant and Madsen (1982) in the modified version of Tolman (1994) is chosen to describe the effects of bottom mobility. The wave and current bottom friction factors appearing in the expressions for the drag coefficient and the bottom mobility parameter are derived from the resistance law for the oscillatory, rough, turbulent BBL which accounts for the usually neglected effects of rotation and the phase difference between the bottom stress and the friction-free current velocity. It is shown that in the fixed-bottom case the drag coefficient is determined by five dimensionless parameters, namely the ratio between the friction-free wave and current velocity amplitudes, the wave and current bottom Rossby numbers, the ratio of the inertial frequency to the representative wave frequency, and the ratio between the wave and current reference bottom roughness lengths. Two additional parameters, the ratio of the representative wave frequency to the buoyancy frequency of suspended sediment particles and the ratio of the mean grain size to the wave reference bottom roughness length must be included in the moveable bottom case.

The above formulation has been implemented in the UCA 2D nonlinear, high-resolution, hydrodynamic model and the advanced model has been applied to quantify changes in the tidal dynamics and energetics of the Cadiz Bay due to wind-wave/tide interaction, bottom mobility and the improved flow-resistance representation. It is found that the inclusion of either of the two first factors causes the drag coefficient to increase several fold over its reference value. Whereas, if the third factor is included, the changes in the drag coefficient are quite moderate. This is because the effect of rotation on the drag coefficient is opposite in sign to the effect of the phase

difference between the bottom stress and the friction-free tidal velocity, so that in aggregate, both effects nearly balance. Inspection of the fields of tidal characteristics reveals that bottom mobility has as important an influence on tidal dynamics as wind-wave/tide interaction has. This is related to large irregular variations in the drag coefficient that accompany sediment motion. Also, it appears that the inclusion of wind-wave/tide interaction, bottom mobility and the improved flow-resistance representation provides a slightly better agreement between the predicted and observed tidal elevation amplitudes and phases than that obtained ignoring these factors.

The formulation considered here rests on a physical similarity between the process of wind-wave/low-frequency current interaction and its real physical analogues in other fields of nonlinear physics (nonlinear optics, nonlinear acoustics and nonlinear radiophysics) where it is regarded as being axiomatic that the interaction between motions with widely different temporal and spatial scales is weak, even though these motions are in themselves strongly nonlinear. As applied to the issue at hand, this rule admits a weak correlation between the bottom stress oscillations with wave and low frequencies and, hence, an adequate description of the overall bottom stress in the combined motion through linear superposition of the wave and current bottom stresses. Clearly, this formulation differs conceptually from formulations in which the interaction between wind waves and low-frequency currents is considered to be strong in the sense that the overall bottom stress is distinct from the sum of the wave and current bottom stresses.

Our formulation differs from other such formulations in specific ways. Among these are the improved flow-resistance representation, the description of the vertical eddy viscosity in the log BBL, which excludes unrealistic discontinuities at the top of the wave BBL, the use of different values of the reference bottom roughness length for the wave and current BBLs, the determination of the wave and current BBL depths, and the means of obtaining the resistance law for the oscillatory, rough, turbulent BBL and parameterizing the effect of suspended sediment stratification (cf., Glenn and Grant, 1987; Alvarez et al., 1999; Kagan et al., 2003b).

Despite these distinctions, the different formulations are all consistent with the same field data (Kagan and Utkin, 2000), although this might be due to a strong scatter in experimental estimates of the drag coefficient. In other words, the data presently available are not sufficiently accurate or reliable to validate any specific formulation of wind-wave/low-frequency current interaction. This opens up the way for other interpretations of the resulting changes in model predictions. For example, as noted by a reviewer, one can conclude that the changes are within the range of uncertainty in the observations, but not associated with the above-mentioned factors at all. As long as the needed data are missing, this interpretation will have the right to its existence, even though it is in contradiction with the predicted changes in the M_4 and M_6 overtides in Cádiz Bay, the changes that appear closely established if wind-wave/tide interaction is accounted for (see Kagan et al., 2003b). Because the required field measurements are unlikely to become available in the near future, the only way out that may be found today is to make up for a deficiency in field and laboratory observations using model-generated data. In so doing various (one- and two-equation) turbulence closure models for the oscillatory, rough, turbulent BBL should be employed to be certain that the results obtained are not model-dependent.

Apart from the fact that a considerable amount of suitable data needs to be available, the formulation of weak-wave/low-frequency current interaction must be improved in some respects. First, as presented the formulation suggests implicitly that the spectral wave-field representation can be replaced by the quasi-monochromatic wave-field representation, i.e., by an equivalent wave with the rms amplitude and the representative (spectrally averaged or spectral-peak) frequency, without any changes in wind-wave forcing. This assumption is valid if the wave orbital velocity in the near-bottom log layer has a narrow spectrum. However, in the case of small depths and/or high wind velocities, it tends to underestimate the bottom stress in the wave BBL

(Kagan, 2003a). How best to revise this formulation is by no means clear.

Second, the resistance law used to evaluate the wave and current bottom friction factors is valid only for heights ranging from the reference bottom roughness length to the top of the relevant BBL. In the moveable-bottom case, this resistance law is applied, following modern practice, to specify the skin friction velocity at the sediment grain roughness length. If the latter is smaller than the wave or current reference bottom roughness length, the resistance law has to be extrapolated outside its range of validity. Errors that may arise from this extrapolation are yet to be estimated.

Third, if the drag coefficient is a discontinuous function of the current bottom Rossby number, which is related to initial ripple formation, a number of additional factors of uncertainty arise in connection with bottom mobility. We mention only one of them. The discontinuous dependence of the drag coefficient on the current bottom Rossby number is responsible for the strong sensitivity of the drag coefficient to the determining parameters, specifically the ratio between the wave and current reference bottom roughness lengths. Therefore, even small errors in setting these lengths will result in inevitable and reasonably large uncertainties in low-frequency current predictions. The magnitude of these uncertainties is unknown.

The last point we wish to discuss concerns applications of the formulation. We have tested it with the UCA 2D hydrodynamic model which, like other 2D models, is incapable of reproducing the vertical profile of velocity unless this profile is specified a priori. Accordingly, the possibility of the formulation quantifying wave-induced changes in the vertical structure of low-frequency flows remains unexplored. In addition, the use of any one 2D model suggests that the friction-free current velocity can be identified with the depth-averaged current velocity. This gives rise to errors in the bottom stress that depend on local water depth in such a manner that as they are larger, the smaller depths are. Therefore, the only way to describe the vertical structure of low-frequency flow and to remove undesirable errors in the bottom stress is to adopt a 3D hydrodynamic model complemented by a proper turbulence closure scheme. Indeed, much needs to be done with respect to theoretical studies of weak wind-wave/low-frequency current interaction.

Acknowledgements

We wish to thank Dr. Alan M.Davies who initiated writing this paper, Dr. T. Weingartner for improving our written English and the reviewers of the paper for their constructive and helpful comments. Financial support was provided by the Russian Basic Research Foundation Grant 04-05-64131.

References

Aldridge, J.N., Davies, A.M., 1993. A high-resolution three-dimensional hydrodynamic tidal model of the eastern Irish Sea. Journal of Physical Oceanography 23, 207–224.

Alvarez, O., 1999. Simulación numérica de la dinámica de marea en la Bahía de Cádiz: análisis de las constituyentes principales, interacción marea-brisa e influencia del sedimento en suspensión. PhD Thesis, Departamento de Física Aplicada, Universidad de Cádiz, Cádiz, Spain, 222 pp.

Alvarez, O., Tejedor, B., Tejedor, L., 1997. Simulacion hidrodinamica en al area de la Baja de Cadiz. Analisis de las constituyentes principales. In: IV Jornadas Espanolas de Puertos y Costas, Servicio de Publicaciones de la Universidad Politechnica de Valencia-98, vol. 2125, pp. 125–136.

Alvarez, O., Izquierdo, A., Tejedor, B., Mananes, R., Tejedor, L., Kagan, B.A., 1999. The influence of sediment load on tidal dynamics, a case study: Cadiz Bay. Estuarine, Coastal and Shelf Sciences 48, 439–450.

Arnskov, M.M., Fredsoe, J., Sumer, B.M., 1993. Bed shear stress measurement over a smooth bed in three-dimensional wave-current motion. Coastal Engineering 20, 277–316.

Bakker, W.T., van Doorn, T., 1978. Near-bottom velocities in waves and a current. In: Proceedings of the 16th International Conference on Coastal Engineering, Hamburg, pp. 1394–1414.

Bender, L.C., Wang, K.-C., 1993. The effect of wave-current interaction on tidally forced estuarine circulation. Journal of Geophysical Research 98, 16,521–16,528.

Bijker, E.W., 1967. Some considerations about scales for coastal models with moveable bed. Publication 50, Delft Hydraulics Laboratory.

Bowden, K.F., 1978. Physical problems of the benthic boundary layer. Geophysical Surveys 3, 255–296.

Cacchione, D.A., Drake, D.E., 1982. Measurements of storm-generated bottom stresses on the continental shelf. Journal of Geophysical Research 87, 1952–1960.

Christoffersen, J.B., Jonsson, I.G., 1985. Bed friction and dissipation in a combined current and wave motion. Ocean Engineering 12, 387–423.

Coffey, F.C., Nielsen, P., 1985. Aspects of wave-current boundary layer flows. In: Proceedings of the 19th International Conference on Coastal Engineering. New York, pp. 22–32.

Davies, A.G., 1990. A model of the vertical structure of the wave and current bottom boundary layer. In: Davies, A.M. (Ed.), Modeling Marine Systems, vol. 2. CRC Press, Boca Raton, Florida, pp. 263–297.

Davies, A.M., Glorioso, P.D., 1999. Near-shore wave-current interaction processes, their effects upon wind driven currents and pollutant transport. In: Moore, C. (Ed.), Coastal Ocean Predictions, vol. 56. AGU Series, Washington, D.C.

Davies, A.M., Lawrence, J., 1994a. Examining the influence of wind and wind-wave turbulence on tidal currents, using a three-dimensional hydrodynamic model including wave-current interaction. Journal of Physical Oceanography 24, 2441–2460.

Davies, A.M., Lawrence, J., 1994b. Modeling the nonlinear interaction of wind and tide: its influence on current profiles. International Journal of Numerical Methods in Fluids 18, 163–188.

Davies, A.M., Lawrence, J., 1995. Modeling the effect of wave-current interaction on the three-dimensional wind driven circulation of the eastern Irish Sea. Journal of Physical Oceanography 25, 29–45.

Davies, A.G., Soulsby, R.L., King, H.L., 1988. A numerical model of the combined wave and current bottom boundary layer. Journal of Geophysical Research 93, 491–508.

Glenn, S.M., Grant, W.D., 1987. A suspended sediment stratification correction for combined wave and current flows. Journal of Geophysical Research 92, 8244–8264.

Grant, W.D., Madsen, O.S., 1979. Combined wave and current interaction with a rough bottom. Journal of Geophysical Research 84, 1797–1808.

Grant, W.D., Madsen, O.S., 1982. Moveable bed roughness in unsteady oscillatory flow. Journal of Geophysical Research 87, 469–481.

Grant, W.D., Williams, A.J., 1985. Reply. Journal of Physical Oceanography 15, 1219–1228.

Grant, W.D., Williams, A.J., Glenn, S.M., 1984. Bottom stress estimates and their prediction on the Northern California continental shelf during CODE-1: the importance of wave-current interaction. Journal of Physical Oceanography 14, 506–527.

Green, M.O., Rees, J.M., King, H.L., 1990. Evidence for the influence of wave-current interaction in a tidal boundary layer. Journal of Geophysical Research 95, 9629–9644.

Gutierrez, J.M., Achab, M., Parrado, J.M., 1996. Distribution of recent facies at the bottom of the Bay of Cadiz. Geogaceta 21, 155–157.

Hasselmann, K., Collins, J.I., 1968. Spectral dissipation of finite depth gravity waves due to turbulent bottom friction. Journal of Marine Research 26, 1–12.

Heathershaw, A.D., 1981. Comparison of measured and predicted sediment transport rates in tidal currents. Marine Geology 42, 75–104.

Huntley, D.A., Hazen, D.G., 1988. Seabed stresses in combined wave and steady flow conditions on the Nova Scotia continental shelf: field measurements and predictions. Journal of Physical Oceanography 18, 347–362.

Kagan, B.A., 2003a. Spectral formulation of weak wind-wave/tide interaction: a quasi-monochromatic approximation. Izvestiya, Atmospheric and Oceanic Physics 39, 240–247.

Kagan, B.A., 2003b. On the resistance law for the oscillatory, rotating, rough, turbulent flow. Izvestiya, Atmospheric and Oceanic Physics 39, 833–837.

Kagan, B.A., Utkin, K.B., 2000. Weak wave-tide interaction and the drag coefficient in a tidal flow. Izvestiya, Atmospheric and Oceanic Physics 36, 566–574.

Kagan, B.A., Tejedor, L., Alvarez, O., Izquierdo, A., Tejedor, B., Mananes, R., 2001. Weak wave-tide interaction formulation and its application to Cadiz Bay. Continental Shelf Research 21, 697–725.

Kagan, B.A., Alvarez, O., Izquierdo, A., Mananes, R., Tejedor, B., Tejedor, L., 2003a. Weak wind-wave/tide interaction over a moveable bottom: results of numerical experiments in Cadiz Bay. Continental Shelf Research 23, 435–456.

Kagan, B.A., Alvarez, O., Izquierdo, A., Mananes, R., Tejedor, B., Tejedor, L., 2003b. Weak wave/tide interaction in suspended sediment-stratified flow: a case study. Estuarine, Coastal and Shelf Sciences 56, 989–1000.

Keen, T.R., Glenn, S.M., 1995. A coupled hydrodynamic-bottom boundary layer model of storm and tidal flows in the Middle Atlantic Bight of North America. Journal of Physical Oceanography 25, 391–406.

Kemp, P.H., Simons, B.R., 1982. The interaction between waves and a turbulent current: waves propagating with the current. Journal of Fluid Mechanics 116, 227–250.

Lou, J., Ridd, P.V., 1997. Modelling of suspended sediment transport in coastal areas under waves and currents. Estuarine, Coastal and Shelf Sciences 45, 1–16.

Lundgren, H., 1973. Turbulent currents in the presence of waves. In: Proceedings of the 13th International Conference on Coastal Engineering. New York, pp. 623–634

Malarkey, J., Davies, A.G., 1998. Modelling wave-current interactions in rough turbulent bottom boundary layers. Ocean Engineering 25, 119–141.

Mathisen, P.P., Madsen, O.S., 1996a. Waves and currents over a fixed ripple bed. 1. Bottom roughness experienced by waves in the presence and absence of currents. Journal of Geophysical Research, 101, 16,533–16,542.

Mathisen, P.P., Madsen, O.S., 1996b. Waves and currents over a fixed ripple bed. 2. Bottom and apparent roughness experienced by currents in the presence of waves. Journal of Geophysical Research, 101, 16,543–16,550.

Mellor, G., 2002. Oscillatory bottom boundary layers. Journal of Physical Oceanography 32, 3075–3088.

Myrhaug, D., 1984. A theoretical model of combined wave and current boundary layers near a rough sea bottom. In: J.C. Chung (Ed.), Proceedings of the Third International Symposium on Offshore Mechanics and Arctic Engineering. Vol. 1. New York, American Society of Mechanical Engineers, pp. 559–568.

Myrhaug, D., Reed, K., Fyfe, A.J., 1987. Sea boundary layer studies for pipelines: large scale laboratory experiments. In: Proceedings of the Third International Symposium on Offshore Engineering, Rio de Janeiro, pp. 345–359.

Signell, R.P., Beardsley, R.C., Graber, H.C., Capotondi, A., 1990. Effect of wave-current interaction on wind-driven circulation in narrow, shallow embayments. Journal of Geophysical Research 95, 9671–9678.

Simons, R.R., Kyriacou, A., Soulsby, R.L., Davies, A.G., 1988. Predicting the near bed turbulent flow in waves and currents. In: Proceedings of the IAHR Symposium on Mathematical Modelling of Sediment Transport in the Coastal Zone. Copenhagen, pp. 33–47.

Simons, R.R., Grass, A.J., Mansour-Tehrani, M., 1992. Experimental study of waves and currents crossing at right angles. In: Proceedings of the 23rd International Conference on Coastal Engineerings. Venice, pp. 604–607.

Sleath, J.F.A., 1990. Velocities and bed friction in combined flows. In: Proceedings of the 22th International Conference on Coastal Engineering. Delft, pp. 450–463.

Smith, J.D., 1977. Modelling of sediment transport on continental shelves. In: Goldberg, E.D., Mc Cave, I.N., O'Brien, J.J., Steele, J.H. (Eds.), The Sea, Vol. 6. Interscience, New York, pp. 539–577.

Smith, J.D., McLean, S.R., 1977. Spatially averaged flow over a wavy surface. Journal of Geophysical Research 82, 1735–1746.

Soulsby, R.L., Humphrey, J.D., 1990. Field observations of wave-current interaction at the sea bed. In: Torum, A., Grudmestad, O.T., (Eds.), Proceedings of the NATO Advanced Research Workshop on Water Wave Kinematics. Kluwer, Dordrecht, pp. 413–428.

Spaulding, M.L., Isaji, T., 1987. Three-dimensional continental shelf hydrodynamic model including wave-current interaction. In: Nihoul, J.C.J., Jamart, B.M. (Eds.), Three-Dimensional Models of Marine and Estuarine Dynamics. Elsevier, New York, pp. 405–426.

Tanaka, H., Shuto, N., 1981. Friction coefficient for a wave-current coexistent system. Coastal Engineering Japan 24, 105–128.

Tang, Y.M., Grimshaw, R., 1996. The effect of wind-wave enhancement of bottom stress on the circulation induced by tropical cyclones on continental shelves. Journal of Geophysical Research 101, 22,705–22,714.

Tejedor, L., Tejedor, B., Alvarez, O., Izquierdo, A., Vidal, J., 1998. Modelo de evaluacion tecnica para la gestion y ordenacion de estuaries. Technical Report, Departamento de Fisica Aplicada, Universidad de Cadiz, Spain, 150pp. Unpublished.

Tolman, H.L., 1994. Wind waves and moveable-bed bottom friction. Journal of Physical Oceanography 24, 994–1009.

Trowbridge, J., Agrawal, Y.C., 1995. Glimpses of a wave boundary layer. Journal of Geophysical Research 100, 20,729–20,743.